International Journal of Engineering Trends and Technology
ISSN: 2231 – 5381 /doi:10.14445/22315381/IJETT-V70I1P208

Volume 70 Issue 1, 63-74, January, 2022

Original Article

PEM Fuel Cell Powered Electric Vehicle Propelled by PMSM Using Fuzzy PID Controller- A Research

Uma Ravi Sankar Yalavarthy[1], Venkata Siva Krishna Rao Gadi [2]

[1]*Research Scholar,*[2]*Professor & HOD, Department of Electrical Engineering, Andhra University, AU North Campus, Visakhapatnam, AP-530003, India*

[1]ysankar.rs@andhrauniversity.edu.in, [2]gvskrishna_rao@yahoo.com

Abstract - *Fuel cells are becoming quite popular these days due to their benefits, such as simplicity, reliability, low pollution, and noiselessness. Despite the numerous flaws in the advancement of fuel cell-based electric vehicles (EV), the objective is to test the accomplishment of Fuzzy PID controlled Permanent magnet synchronous motor (PMSM) propelled electric vehicle powered by proton exchange membrane (PEM) fuel cell in terms of control design and motor drive mechanism. In this paper, the dynamics of electric vehicles are considered, and space vector pulse width modulation (SVPWM) converter control methodology is employed. This research provides a Fuzzy PID controller-based control approach for different motor-loaded conditions, and it is compared with a classical PID controller. The system is modeled and simulated in Matlab/Simulink environment. The control strategy was found to be effective based on the outcomes. The findings confirm that the PEM fuel cell electric vehicle's control technique is effective and efficient throughout a vast speed range.*

Keywords — *electric Vehicle (EV), permanent magnet synchronous motor (PMSM), Proton exchange membrane (PEM), space vector pulse width modulation (SVPWM).*

I. INTRODUCTION

There is indeed a rising need for ecological automobiles all around the world, and this demand is likely to expand dramatically in the coming years, and so severe emissions regulations are enforced. The objective of such limitations is to achieve zero particulate discharges and carbon dioxide abatement; therefore, it is not astonishing that demand for greener, zero-emission sources of energy is surging. EVs are one of the options to the ever-increasing need for cleaner automobiles, and so they are incredibly effective, emit zero emissions, are quieter [1]. All vehicle manufacturing firms are currently grappling with energy and environmental challenges. Producing clean energy vehicles are the current fashion for personal mobility [2]. The demand for environmental preservation and depletion of the earth's oil reserves have led to the consideration of electric vehicles as one of the feasible alternatives. EV technology, when compared to traditional automobiles, offers an excellent option towards obtaining superior performance [3].

For well over a decade, researchers have been studying the fuel cells for their use in automobiles [4]-[7]. Nowadays, Fuel cells have attracted growing interest as a possible renewable energy source due to their low ecological damage. In the fuel cell, hydrogen and oxygen combine in the presence of a catalyst and get transformed into water and heat. This electro-chemical process results in the production of electric energy [8], [9]. The PEM fuel cell has gained significant interest in the past couple of decades because of its numerous benefits. Rapid response, High power density, good overall efficacy, negligible exhaust discharges, inexpensive, less operational temperature, and quick start-up are only a few of features [10]. As a result, PEMFCs are regarded as the hopeful prospects for upcoming energy production equipment, specifically mobility, home electricity production, and wearable digital devices [11], [12].

The PEMFC EV battery power systems are investigated in this work, where the FC serves as a prime energy provider, whereas the Li-ion cell serves as the supplementary energy supplier. Li-ion batteries have a huge capacity, less price, and a vast number of cycles for charging and discharging relatively to all other types of battery cells [13], [14]. The fuel cell provides power to charge until the Li-ion battery achieves a higher state of charge (SOC). The fuel cell is linked to a DC/DC unidirectional boost converter, which is subsequently connected to the DC bus. Then, a Li-ion battery is immediately connected to the DC bus, sustaining the bidirectional flow of power. The benefits mentioned so far are the primary factors why fuel cell battery units are extensively used in EVs.

PMSM is commonly employed to propel automobiles these days. Because of PMSM's remarkable qualities, which include great efficiency, high torque to volume proportion, and power factor and so it is recognized as a worthy choice for EVs [15] - [17]. The power conversion systems consisting of a DC/DC boost converter as well as an SVPWM inverter provide power from the fuel cell to the PMSM. Due to their lower generated output voltage, DC/DC boost converters were the highest preferred equipment used in PEM fuel cell systems. While dealing with the PMSM drive system, traditional control strategies PI and PID

were often employed. These control techniques could be more effective for linear systems. Moreover, because of the nonlinearity of the PMSM drive system, it is hard to analyze system parameter fluctuations. A fuzzy-based PID controller is regarded as one of the best methods for controlling dynamic non-linear systems. As a result, the dynamic system response is improved. Moreover, the fuzzy PID controller is well-known as a reliable control mechanism for handling complex systems.

This research sought to investigate fuzzy PID controlled space vector modulation inverter-based indirect vector control, which regulates the PMSM to reduce speed and torque irregularities. The drive parameters are automatically corrected, and indeed the governing rules are refined in response to load variations of the PMSM during the actual functioning of the PEM fuel cell electric vehicle. Modeling of the propulsion system is required for a piece of complete knowledge about vehicle dynamics. The dynamic model of the system is designed and simulated in MATLAB/SIMULINK at different loading circumstances. The simulation results are provided and confirmed for the system under various operating scenarios.

The paper is structured; section I of this paper introduces the work. Section II contains all of the EV dynamic modeling formulations. Section III discusses the mathematical modeling of indirect space vector control of PMSM drive and SVM inverter. Section IV discussed the fuzzy PID controller. Section V dealt with PEMFC, DC-DC boost converter, and battery. Finally, in section VI, the simulation results of various driving circumstances are displayed and followed by a conclusion in section VII at last.

II. ELECTRIC VEHICLE DYNAMIC MODEL

ICE vehicles must adhere to a mass-to-power proportion, and electric vehicles must do the same. As a result, the tractive effort F_T (N) must be estimated first in order to construct and evaluate an EV, as shown in Fig. 1.

$$F_T = F_r + F_a + F_h + F_{acc} + F_\omega \tag{1}$$

Where F_r is the force due to rolling resistance, F_a is the force due to aerodynamic drag, F_h is uphill ascent force, F_{acc} is the force necessary to accelerate and F_ω Is the force necessary for angular acceleration.

Where μ_r Is rolling resistance coefficient, g is gravity acceleration (m-s^{-2}), and m is vehicle mass (kg).

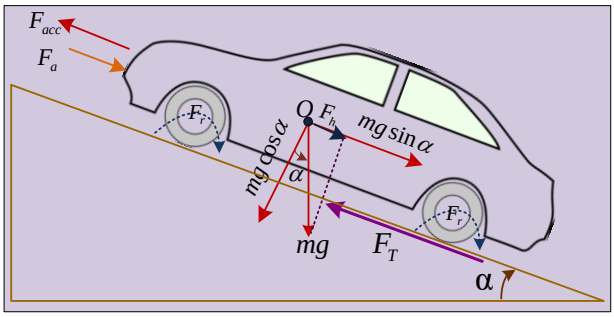

Fig. 1. Forces exerted upon the vehicle

$$F_r = \mu_r mg \tag{2}$$

The vicious opposition of the air blowing on the vehicle is characterized as aerodynamic drag, F_a.

$$F_a = \frac{1}{2}\rho C_d A V^2 \tag{3}$$

Where C_d Is drag coefficient, approximately 0.2, ρ is the density of air (kg.m^{-3}), V is vehicle speed (m-s^{-1}), and A is the frontal area (m^2).

The uphill force is considered as positive during ascent and negative during descent for grading angle α.

$$F_h = mg\sin\alpha \tag{4}$$

Applying Newton's second law, the accelerating force of the vehicle is given in Eq. (5).

$$F_{acc} = ma \tag{5}$$

Where a is the acceleration of the vehicle (m-s^{-2}), it is also vital to include the force required to make the revolving part meet the desired speed and torque requirements for a more realistic representation. As a result, the angular acceleration is given in Eq. (6).

$$F_\omega = \frac{I}{\eta_g}\left(\frac{G}{r}\right)^2 a \tag{6}$$

Where η_g The efficiency of the gear ranges from 0.84 – 0.96, G is the gear ratio, I is a motor moment of inertia (kg-m^{-2}), and r is the radius of wheel (m).

III. DESIGN OF PMSM DRIVE

A. Mathematical modeling of PMSM

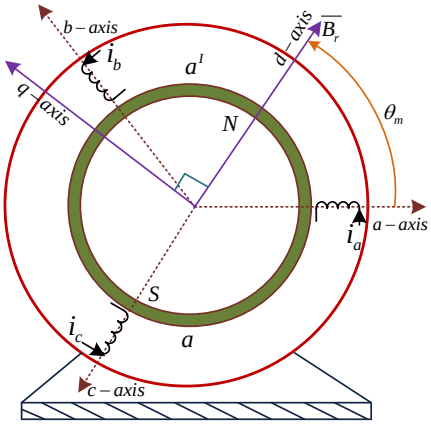

Fig. 2. Structure of permanent rotor magnet and stator 3-φ windings of PMSM

The stationary reference frame makes it difficult to analyze and solve synchronous motors because they contain a set of non-linear equations. So, as per the vector transformation theory, the PMSM model in a coordinate system of the synchronous rotating frame is shown in Fig. 2. The rotor in PMSM with surface-mounted permanent magnets could be regarded as magnetically round, having the same reluctance along any axis through the machine's center. The magnetic field developed by both the permanent magnet and stator 3-φ winding is assumed to be spatially sinusoidal.

The PMSM drive model is a two-loop system with a current-loop considered as an inner loop and a speed-loop considered as an outer loop. Vector transformation has become one of the most popular schemes for the mathematical framework of PMSM in recent times.

The CLARK and PARK transformation could transform 3-φ parameters in the abc frame to 2-φ parameters in the dq frame [18], [19]. The principle of operation of PMSM is similar to that of the torque control strategy implemented in DC motors. The stator direct axis current i_d^* is kept zero, whereas the stator quadrature axis current i_q^*Is responsible for the speed control of PMSM. The fuzzy logic-based PID controller in the speed-loop generates the q-axis reference current i_q^*, when the actual rotor speed ω_r is compared with the reference speed ω_r^* With the help of a comparator. The PI controllers present in both dq channels generate the reference dq voltages v_d and v_qFrom reference stator dq currents. These reference voltages are fed to an SVPWM inverter to generate the regulated dq voltages that are directed to the PMSM stator windings for control action. The PMSM dynamic equations are given in Eq. (7) [20].

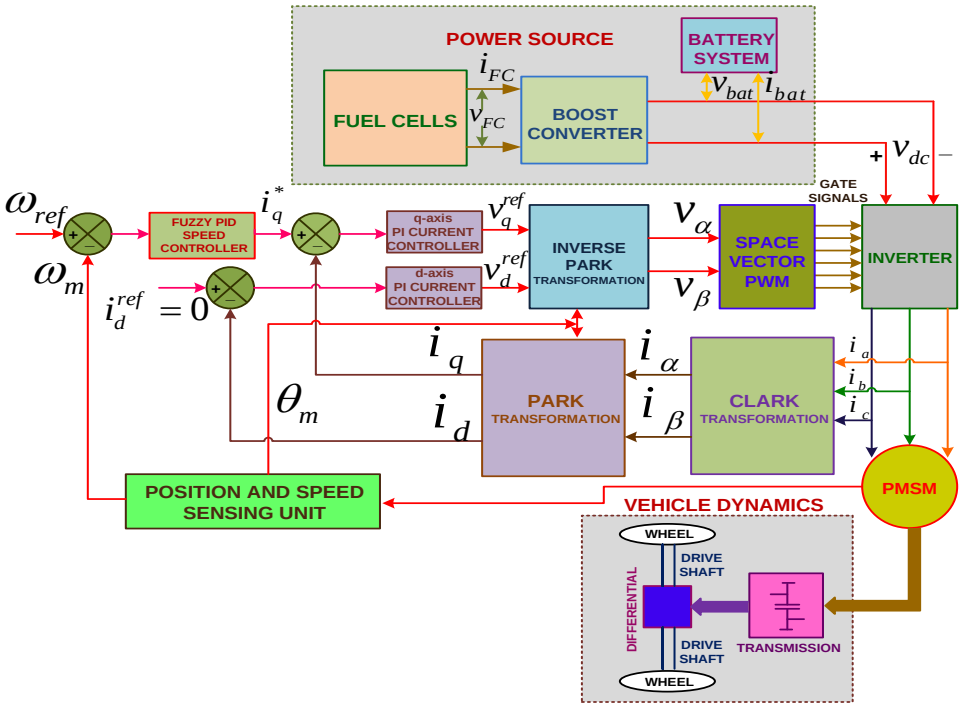

Fig. 3. Vector control of fuel cell fed Electric vehicle functional diagram

$$\left.\begin{aligned}
\frac{d}{dt}i_d &= \frac{v_d - Ri_d + \omega_r L_q i_q}{L_d} \\
\frac{d}{dt}i_q &= \frac{v_q - Ri_q + \omega_r L_d i_d - \omega_r \psi_f}{L_q} \\
\frac{d}{dt}\omega_r &= \frac{\tau_e - \tau_l - B_r\omega_r}{J} \\
\frac{d}{dt}\theta_r &= \omega_r \\
\omega_m &= \omega_r.\frac{2}{p} \\
\tau_e &= \frac{3}{2}p\left[\psi_f i_q + (L_d - L_q)i_d i_q\right]
\end{aligned}\right\} \quad (7)$$

Where i_d and i_q are the stator direct and quadrature axis currents in the dq frame of reference. R is the phase resistance of stator (Ω), v_d and v_q Are the stator direct and quadrature axis voltages in the dq frame of reference. B_r Is rotor flux density (Wb-m^{-2}). ω_r, ω_m and θ_r Are the rotor electrical speed, rotor mechanical speed, and angular position, respectively (rad-s$^{-1,}$ rad-s^{-1}, rad). τ_e and τ_l is the electromagnetic torque and load torque, respectively (N-m). J is the combined inertia of load and motor (kg-m^2), and p is the pole number.

B. Modelling of SVPWM inverter

When compared to sinusoidal PWM, SVPWM is the advanced way to design a basic sine wave that offers greater voltage at stator windings of PMSM and reduces total harmonic distortion. For SPWM the developed voltage is given in Eq. (8) [21], [22].

$$\left|\overrightarrow{v_{s(max)}}\right|_{L-L(rms)} = \frac{\sqrt{3}v_{dc}}{2\sqrt{2}} = 0.612v_{dc} \quad (8)$$

For SVPWM, the developed voltage is given in Eq. (9)

$$\left|\overrightarrow{v_{s(max)}}\right|_{L-L(rms)} = \frac{v_{dc}}{\sqrt{2}} = 0.707v_{dc} \quad (9)$$

On comparing Eq. (8) and Eq. (9), the available voltage at the output is 15% more in the case of SVPWM methodology.

The basic circuital of the SVPWM converter is depicted in Fig. 4. It comprises of DC voltage source, poles a, b, and c with switches Q_a, Q_b, and Q_c. On the basis of their ON and OFF positions, logic 1 and 0 are ascribed to the switches. Q_c, Q_b, and Q_a make up a 3-bit notation, resulting in six basic vectors and two zero vectors.

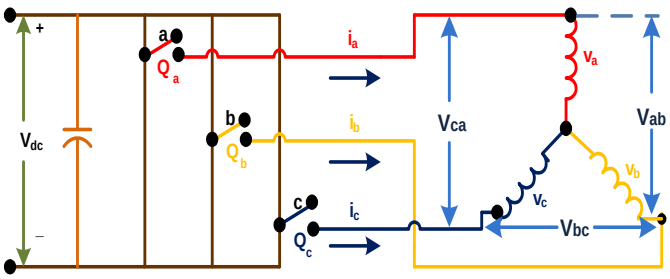

Fig. 4. The basic circuit of the SVPWM inverter

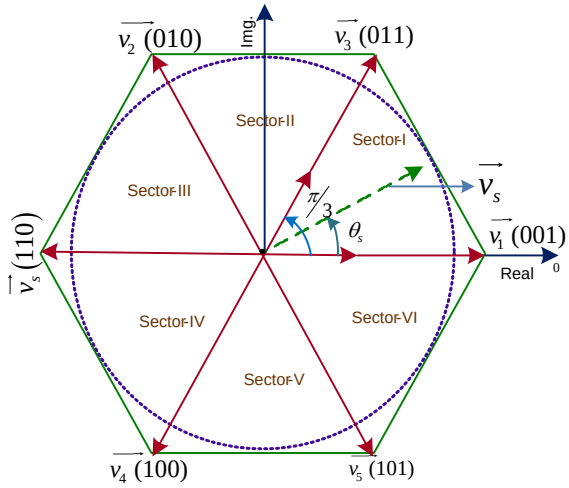

Fig. 5. Sectors and basic vectors representation

The main purpose of this technique is to produce proportionate stator output three-phase voltages with respect to reference signals. In the implementation of SVPWM, the 3-φ voltage vectors get transformed to 2-φ voltage vectors, as an outcome space vector from $\overrightarrow{v_0}$ to $\overrightarrow{v_7}$ Are available as depicted in fig. 5. $\overrightarrow{v_1}$ to $\overrightarrow{v_6}$ are basic vectors and $\overrightarrow{v_0}$, $\overrightarrow{v_7}$ Are zero vectors. Each pole should change its position once in each switching period T_S for SVPWM to obtain a steady switching frequency and best harmonic response. To establish the largest magnitude of the voltage at the output of stator voltage space vector $\overrightarrow{v_s}$, combine the ends of the basic vectors to construct a hexagon. The largest magnitude of voltage is given in Eq. (9). Fig. 21 depicts the control voltages developed by the SVPWM inverter. The gate signals are generated by comparing control voltages with the triangular voltage signal for a given DC voltage. These signals are given to a three-phase inverter to develop stator three-phase voltages and currents as shown in Fig. 21, 22. [23]

IV. PID CONTROLLER BASED ON FUZZY LOGIC

A. Concept of PID Control

PID control essentially means regulating the three proportional, integral, and differential constants denoted by K_P, K_I and K_D Respectively. The controller's response

expression is shown in Eq. (10).

$$error\ (e) = output - input$$
$$u(t) = K_P e(t) + K_I \int e(t)\,dt + K_D \frac{de(t)}{dt} \qquad (10)$$

Modify the PID controller specifications to fit the design criteria, resulting in an improved steady and transient behavior for the controlled object. Fig. 6(a) depicts the actual PID control design.

a) Proportional Term:

Governing and lowering bias through altering the design control proportionally to that same level of bias. The function of the scaling factor is to enhance the time by the system to respond. A higher value of scaling factor implies the quicker the response and vice-versa.

b) Integral Term:

It is employed to get rid of steady-state errors and enhance the system error rate. The degree of an integral connection is governed by the integral time constant, and however, if the integral activity is so powerful, it will impact the system's stability.

c) Differential Term:

This would change the system control quantity based upon that variability tendency of deviated quantity. A corrective signal is provided prior to a significant shift in the deviated signal that could accelerate the system operating speeds and minimize the control time. It is important to keep in mind when adjusting the differential factors because so much differential activity can create system oscillation.

It seems to be easy to understand that the PID controller set of parameters would be the basic fundamental of the PID control scheme. In traditional PID control, the PID parameters are a collection of preset values [24].

B. Fuzzy PID Control

Classical PID controllers lack the ability to make real-time variable improvements and cannot handle the tough situations of a fuel cell electric vehicle. Here PID control with an adaptive fuzzy logic mechanism is implemented. Consider a speed control loop shown in Fig. 6(b).

On comparing reference speed with actual speed, the speed error e is obtained. Let de/dt Is the rate of change in speed error. To begin, initialize the proportional, integral, and derivative constants K_{PO}, K_{IO} and K_{DO} Respectively. The e and de/dt undergo three stages, namely fuzzification, inference, and defuzzification to obtain the compensation in constants $\Delta K_P, \Delta K_I$ and ΔK_D. By combining the original and compensation terms in Eq. (11), the control terms K_P, K_I and K_DCan be obtained [25].

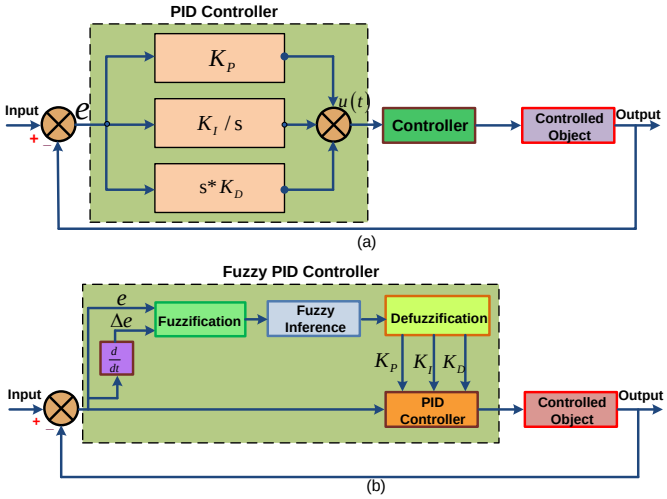

Fig. 6. (a) PID controller structure (b) Fuzzy PID Controller

TABLE I. RULE BASE FUZZY CONTROL

e / Δe	nh	nm	nl	ze	pl	pm	ph
nh	ph nh pl	ph nh pl	pm nh ze	pm nm ze	pl nm ze	pl ze ph	ze ze ph
nm	ph nh nl	ph nh nl	pm nm nl	pm nm nl	pl nl ze	ze ze pl	ze ze pm
nl	pm nm nh	pm nm nh	pm nl nm	pl nl nl	ze ze ze	nl pl pl	nm pl pm
ze	pm nm nh	pl nl nm	pl nl nm	ze ze nl	nl pl ze	nm pl pl	nm pm pm
pl	pl nl nh	pl nl nm	ze ze nl	nl pl nl	nl pl ze	nm pm pl	nm pm pl
pm	ze ze nm	ze ze nl	nl pl nl	nm pm nl	nm pm ze	nm ph pl	nh ph pl
ph	ze ze pl	nl ze ze	nl pl ze	nm pm ze	nm ph ze	nh ph ph	nh ph ph
nh=negative high		nm=negative medium		nl=negative low		ze = nearly zero	
pl = positive low		pm=positive medium		p = positive high			

$$\left.\begin{aligned} K_P &= K_{PO} + \Delta K_P \\ K_I &= K_{IO} + \Delta K_I \\ K_D &= K_{DO} + \Delta K_D \end{aligned}\right\} \qquad (11)$$

The self-tuning control system can be accomplished by repeatedly comparing the reference and actual speeds to obtain e and de/dt Which can then be used to adapt the control variables. Here, the triangle membership function is used by the fuzzy controller. All of the membership functions are symmetrically allocated. For defuzzification, a weighted average approach is utilized [26].

A fuzzy set is taken as {nh, nm, nl, z, pl, pm, ph}, input has discourse universe of [-4, 4], output has discourse universe for K_P, K_I and K_D are [-0.4, 0.4], [-0.08, 0.08] and [-4, 4] respectively. According to the fuzzy control rule base, rules are put together for K_P, K_I and K_D From top to bottom, as shown in Table I.

V. DESIGN OF PEM FUEL CELL

A. Fuel Cell Model

Depending on their unique characteristics, fuel cells are a great option for electric vehicle applications [27]. A fuel cell directly converts chemical energy into electricity. As depicted in Fig. 7, fuel hydrogen enters into the fuel cell from the left side, whereas oxygen from the atmosphere enters from the right. Accompanying catalyst, hydrogen atom splits into hydrogen ions and electrons. These ions combine with oxygen to form water and heat. Electrons that enter the cathode are in charge of producing electric energy. The chemical changes that occur at the anode and cathode are listed below in Eq. (12).

As a result, the PEM fuel cell supplies electricity to load. In contrast to a battery, the matter consumed in the process of electrochemical reaction is constantly replenished, so the fuel cell is not required to be recharged.

$$\left.\begin{aligned} At\ anode\ H_2 &\leftrightarrow 2H^+ + 2e^- \\ At\ cathode\ 2H^+ + \frac{1}{2}O_2 + 2e^- &\leftrightarrow H_2O \\ H_2 + \frac{1}{2}O_2 &\leftrightarrow H_2O + Electric\ Energy \end{aligned}\right\} \quad (12)$$

With the assistance of hydrogen gas and atmospheric oxygen, fuel cells (FCs) can generate electricity with good efficiency, reduced processing noise, and zero emissions. PEM fuel cells are a kind of fuel cell that is primarily built for electrical vehicles. They are mainly devised for road transport, along with static and compact fuel-cell implementations [28]-[30]. Lower temperature and pressure span with a peculiar proton-conducting polymer electrolyte layer differentiate them

PEM fuel cells generate electric energy and work on the inverse concept of PEM electrolysis, which utilizes electricity. They are a strong contender to replace aging alkaline fuel-cell innovation. The voltage output v_{fc} In a PEM fuel cell is given by Eq. (13) [31]. The terms description of Eq. (13) is given in Table II.

The voltage developed in the fuel cell is less. So, N numbers of fuel cells are put together in series. The net voltage v_{FC} is given in Eq. (14) [32]

$$v_{FC} = N.v_{fc} \quad (14)$$

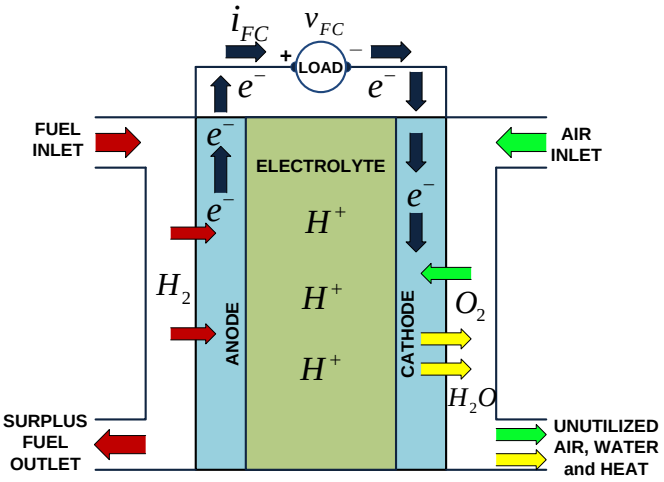

Fig. 7. Fuel cell internal structure

$$\left.\begin{aligned} v_{fc} &= E_{cell} - v_{act} - v_{con} - v_{ohm} \\ E_{cell} &= -\frac{\Delta G}{2F} + \frac{\Delta S}{2F}(T - T_{ref}) \\ &\quad + \frac{RT}{2F}\left(ln(P_{H_2}) + \frac{1}{2}ln(P_{O_2})\right) \\ v_{act} &= \xi_1 + \xi_2.T + \xi_3.T.ln(C_{O_2}) + \xi_4.T.ln(I) \\ v_{con} &= B.ln\left(1 - \frac{J}{J_{max}}\right) \\ v_{ohm} &= I.(R_m + R_c) \end{aligned}\right\} \quad (13)$$

TABLE II. TERMS DESCRIPTION

Symbol	Description
E_{cell}	Open circuit voltage (V)
v_{act}, v_{con} and v_{ohm}	Polarization losses in the fuel cell (V)
F	Faraday's constant
ΔG	Gibbs energy reaction change
ΔS	entropy reaction change
P_{H_2}	Hydrogen partial pressure
P_{O_2}	Oxygen partial pressure
T	Operating temperature
T_{ref}	Reference temperature
C_{O_2}	Concentration of oxygen
ξ_1, ξ_2, ξ_3 and ξ_4	Parametric coefficients
R_m	Electron flow Equivalent resistance (Ω)
R_c	Proton Resistance (Ω)
J	Current density (A.m^{-2})
B	Cell type specific parameter.

B. DC-DC Boost Converter Model

The boost converter raises the potential of the fuel cell to the potential of the battery. Because fuel cell potential and current vary with the requested load power. A DC/DC boost converter connecting the fuel cell to the DC bus is needed to make sure of dynamic output power levels. The role of the boost converter is to ensure the potential of the fuel cell to match with the potential of the battery. The circuitry schematic for the boost converter is shown in Fig. 8, which comprises the inductor (L), capacitor (C), switching element (S), and diode (D) [33].

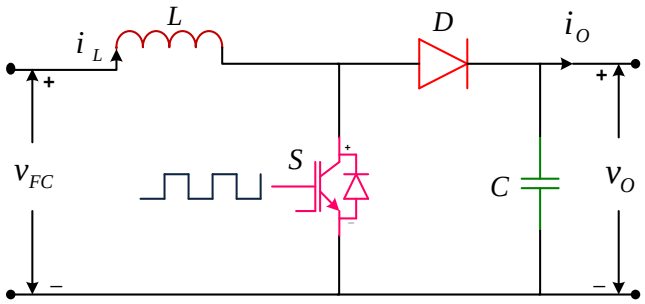

Fig. 8. Boost electric converter circuitry

The relation for voltage developed in fuel cell v_{FC} and boost converter enhanced voltage v_o is given in Eq. (15).

$$v_o = \left[\frac{1}{1-S}\right] v_{FC} \tag{15}$$

Two different system operation scenarios are depicted in Eq. (16) and (17) according to the ON and OFF positions of the switch.

$$for\ S = 1 \quad \begin{cases} \frac{d}{dt} i_o = \frac{1}{L} v_{FC} \\ \frac{d}{dt} v_o = \frac{1}{C}(-i_o) \end{cases} \tag{16}$$

$$for\ S = 0 \quad \begin{cases} \frac{d}{dt} i_o = \frac{1}{L}(v_{FC} - v_o) \\ \frac{d}{dt} v_o = \frac{1}{C}(i_{FC} - i_o) \end{cases} \tag{17}$$

C. Battery

A battery is a device that may be electrically charged to produce a constant voltage for power or discharged to provide an electric current as required. This works under the principle of electrochemical conversion of energy. The basic components of a battery are the anode, cathode, and electrolyte. The most commonly used batteries are Li-ion, Lead-acid, metal-H_2Ni, Ni-Cd batteries. The selection of the battery depends upon the battery's individual characteristics. Lithium-ion batteries are extensively utilized in mobile phones, computers, and EVs for their benefits like low rate of self-discharge, stability, safety, better energy density, and specific energy compared to conventional batteries [34]. To meet the load's power management requirements, the battery employed in transportation applications should be appropriately modeled. The efficacy of an electric vehicle battery is affected by temperature, state of charge (SOC), and charge/discharge current. The battery's SOC is computed by Eq. (18) [35], [36].

$$SOC(t) = SOC_o - \int_0^t \frac{i_{bat}(t)}{Q} \tag{18}$$

Where i_{bat} And Q are the current and maximum capacity of the battery, respectively.

VI. EV SIMULATION, RESULTS, AND DISCUSSION

The vector control method based on fuzzy PID controller-driven PMSM was utilized to verify that the layout of the PEM fuel cell-powered EV has adequate dynamic and static capabilities. During various operating conditions, a MATLAB/Simulink modeling of the comprehensive EV system is constructed and examined. Fig. 9 shows a thorough Simulink model of the proposed vector control method for the entire EV system of Fig. 3. To develop a simulation model, one such model incorporates the concept of segmented simulation, which divides the overall control system into segments. Fig. 10 shows the Simulink model of the PEM fuel cell subsystem. Simulink model of the boost converter is depicted in Fig. 11. The fuzzy PID controller Simulink model is depicted in Fig. 12. The following parameters shown in Table III and Table IV are considered in the dynamic modeling of EV and PMSM drive, respectively.

The PEM fuel cell is constituted of 42 cells that have a peak power of 6 kW. At a pressure and temperature of 0.6 bar and 32°C, respectively, hydrogen fuel is delivered into the fuel cell. Then PEM fuel cell unit meets load requirements, and thus the developed voltage of the boost converter is almost equivalent to 200V.

TABLE III. EV DYNAMIC PARAMETERS

Parameter, Symbol	Value (dimension)
Mass of Vehicle, m	1000 kg
Gravity acceleration, g	9.8 m.s^2
Front Area, A	2.5 m^2
Rolling Resistance Coefficient, μ_r	0.005
The radius of the wheel, r	0.29 m
Aerodynamic coefficient, C_d	0.2
Density of air, ρ	1.3 kg.m^{-3}
Gear Ratio, G	0.95
The efficiency of gear, η_g	0.9
Grading angle, α	0

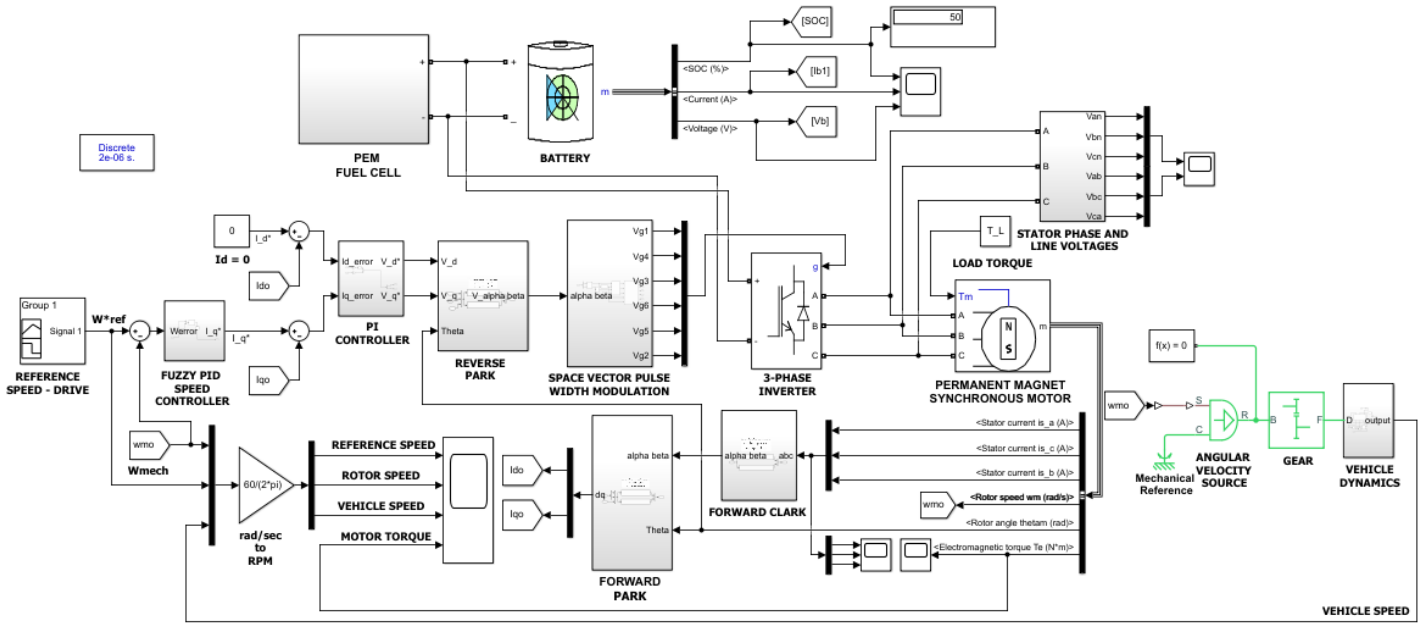

Fig. 9. Simulink model of vector controlled fuel cell fed Electric vehicle

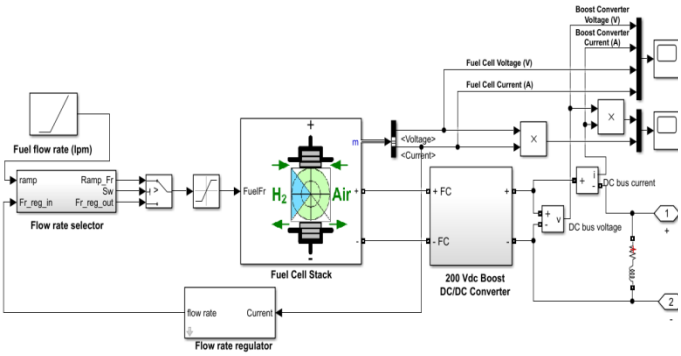

Fig. 10. PEM fuel cell Simulink model

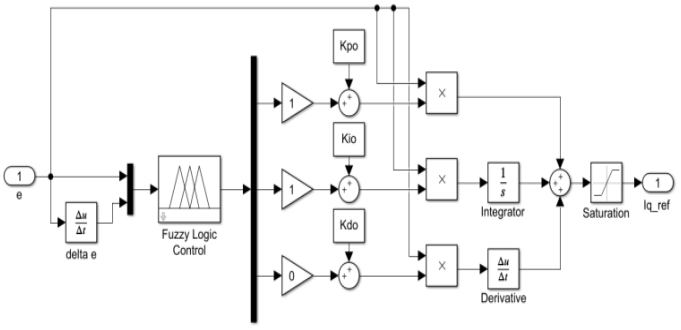

Fig. 12. Simulink model of fuzzy PID controller

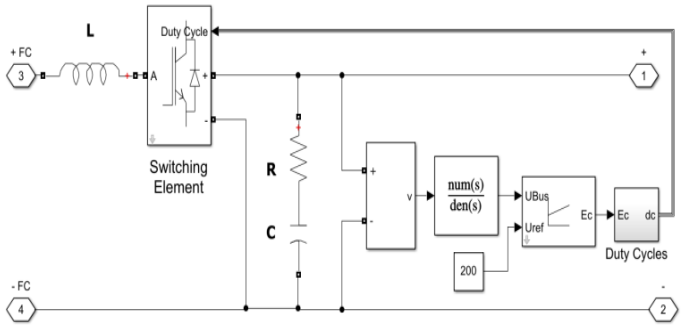

Fig. 11. DC-DC Boost converter simulink model

TABLE IV. PMSM AND SVPWM INVERTER PARAMETERS

Parameter, Symbol	Value (dimension)
Power rating	6 kW
Voltage rating	200 V
Current rating	30 A
Rated Speed	5000 RPM
Phases	3
Torque Rated	40 N-m
d, q axes inductance L_d, L_q	4.6 mH, 10.4 mH
Stator Resistance, R	1.54 Ω
Magnetic flux, ψ_f	0.08127 V-s
Number of poles, p	4
Moment of inertia, J	$1.474X10^{-4}$ kg-m^2
Switching Frequency, f_{SW}	10 kHz
Reference triangular voltage, V_{tri}	5 V
Battery Voltage, V_{dc}	200 V

.

For proper validation of fuzzy PID control methodology, place specifications for PID speed loop controller to $K_P = 90, K_I = 25, K_D = 0.05$, and also place specifications for PI current loop controller to $K_P = 110, K_I = 25$. By considering the above parameters, the fuzzy-based indirect space vector control method of PMSM drive powered by is implemented. A long-span speed reference drive was chosen, and responses were studied under various operational conditions such as trapezoidal, staircase, step, and uneven patterns.

In the perspective of the execution strategy of indirect control of PMSM, holding $i_d = 0$, and the fuzzy PID speed controller supplies the q-axis current according to the requirement. The q-axis reference current is approximated from the torque equation given in Eq. (7). The error current signals generated in dq channels are directed to the PI controller to generate the necessary quadrature voltages. Further, these voltages undergo reverse park transformation and then finally to the SVPWM unit to generate gate signals. These gate signals are given to the inverter to generate the required stator three-phase voltages. Fig. 9 depicts the Simulink model of the above-proposed system.

For every electric vehicle validation, driving the motor in compliance with the nominal speed is essential. Simulating the above system under both conditions, namely steady speed altering torque and steady external torque altering speed, determines the validity of the system.

The simulation is performed for a period of 0.6s in the condition of steady speed altering torque operation. An initial value of control torque is fixed at 10 N-m at a steady speed reference of 50 RPM, and then a step control torque of 20 N-m is imposed at time 0.4 s. In the operation of PMSM under the Fuzzy PID control strategy, at 0.4s, the speed drops from 50 RPM to 45 RPM and returns to its command value in less than 0.1s, as shown in Fig. 13. Whereas in classical PID control of the operation, at 0.4s, the speed drops to 40 RPM and returns to its command speed in 0.15s. It is also observed that the level of overshoot and undershoot in torque profiles is more in the case of conventional PID control scheme of operation. It is quite worth noting that the torque developed by fuzzy PID-controlled PMSM is consistent with the reference step torque, with a torque recovery time of 0.05s.

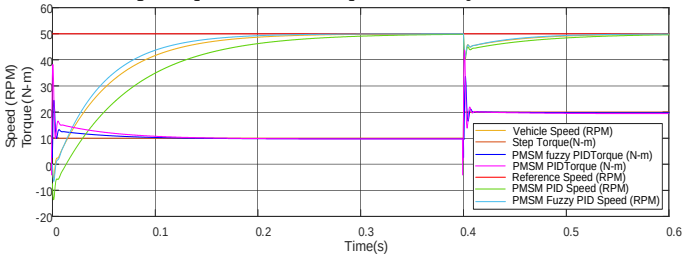

Fig. 13. Speed and torque responses for steady speed altering torque operating condition

The driving curve is defined for a long-span speed control reference drive for a time period of 6 s in the condition of steady torque altering speed functioning of the system, as shown in fig. 14. Under this state, the external torque is fixed at zero throughout the simulation period. The reference speed drive incorporates a staircase speed, step, trapezoidal, and uneven pattern signals for intervals of [0.1, 1.3s], [1.5, 2.3s], [1.8, 2.8s], and [4.5, 6s] respectively, as depicted in Fig. 14. Fig. 15, 16, 17, and 18 show magnified images of Fig. 14 for staircase, step, trapezoid, and uneven speed pattern responses. From Fig. 24, it is evident, to steer the speed of the vehicle in accordance to reference speed-drive, the d-axis current is maintained approximately at zero, whereas the q-axis current regulates the speed of the PMSM.

The PMSM and vehicle speed responses track the commanded speed with zero speed error and stabilize rapidly over frequent speed variations of the entire time period. This really is particularly noticeable when staircase and stepped speed signal inputs are adapted. When a fuzzy PID speed controller is utilized, the response time of PMSM and EV are 0.25s and 0.3s, respectively, to track the reference speed. However, when a conventional PID speed controller is used, it takes 0.45s. Thus, in terms of quick responsiveness, the fuzzy PID outperforms.

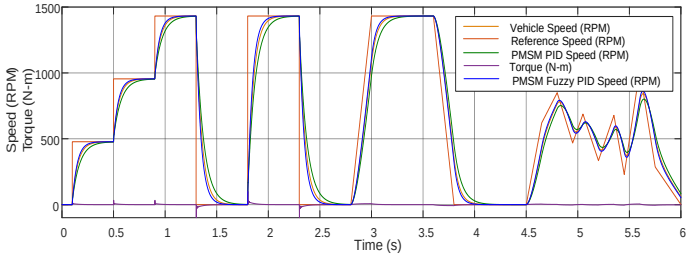

Fig. 14. Speed and torque responses for steady torque and altering speed operating condition

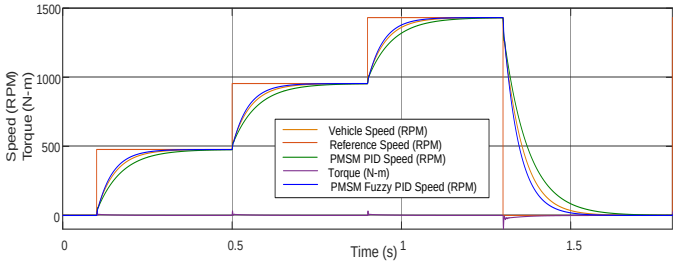

Fig. 15. Stair-case command speed responses magnified image

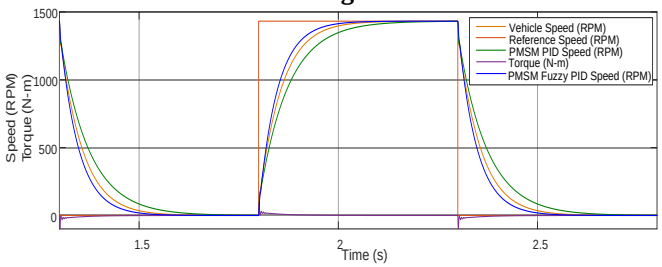

Fig. 16. Step command responses magnified image

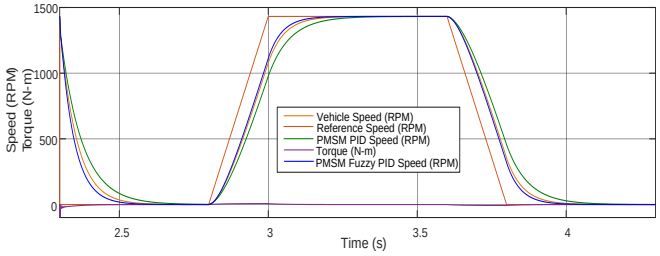

Fig. 17. Trapezoidal command speed responses magnified image

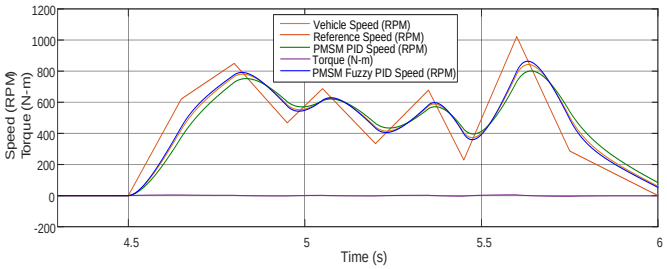

Fig. 17. Uneven pattern command speed responses magnified image

Fig. 18 shows the V-I and P-I characteristics of the PEM fuel cell. It was found out that the average DC output voltage available at its terminals is equal to 51.1 V, and the power produced by the fuel cell steadily grows to MPP as the current increases. The V-I and P-I characteristics of a boost converter are included in Fig. 19. The average voltage output accessible at load terminals equals 200 V, and as the current rises, the power developed by the fuel cell progressively advances to the MPP. Fig. 20 depicts the fuel cell and boost converter voltages under ideal conditions, the PEM fuel system in conjunction with boost converter meets the system load requirements, and the resulting boost converter potential was pretty much equal to 200V.

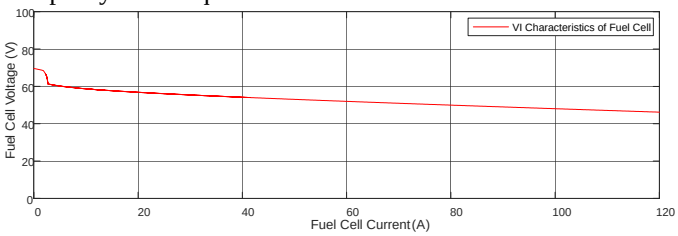

(a)

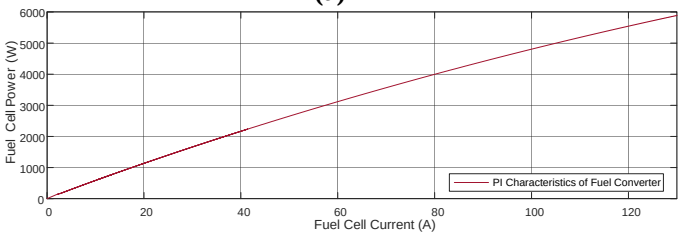

(b)

Fig. 18. V-I and P-I characteristics of PEM Fuel Cell

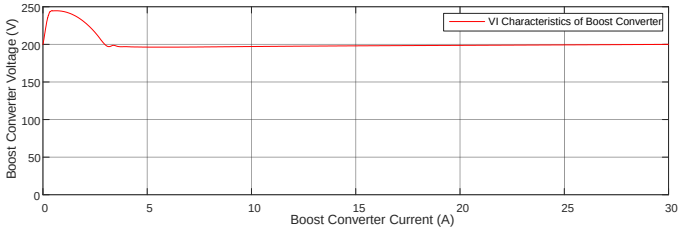

(a)

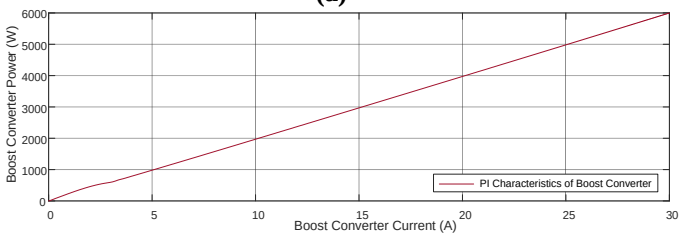

(b)

Fig. 19. V-I and P-I characteristics of Boost Converter

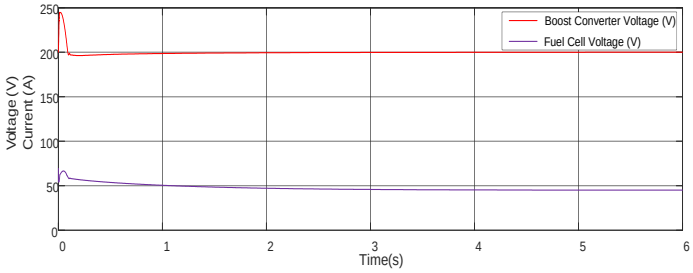

Fig. 20. PEM fuel cell, boost converter output voltages

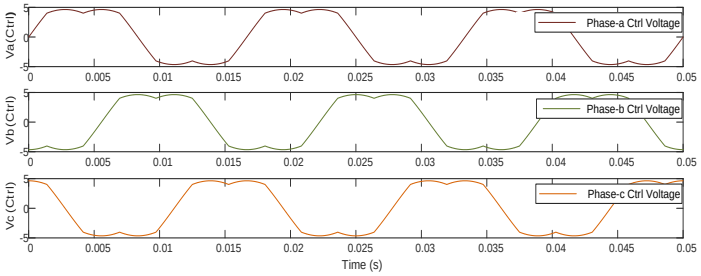

Fig. 21. Control voltages developed by SVPWM inverter

This project makes use of a lithium-ion battery. The battery specifications are as follows, nominal discharge current I is 30 A, internal resistance R is 0.0133 Ω, the capacity of the battery at rated voltage is 46 Ah, cut-off voltage is 150 V, open-circuit voltage E_o Is 204.5 V. The battery voltage remains constant in the nominal area, gradually decreasing over time, as shown in Fig. 25(a) and 26(a). Figure 25(b) and 26(b) depicts battery voltage versus ampere-hour and battery voltage versus time characteristics, respectively, for various discharge currents of 6.5, 13, and 32.5.

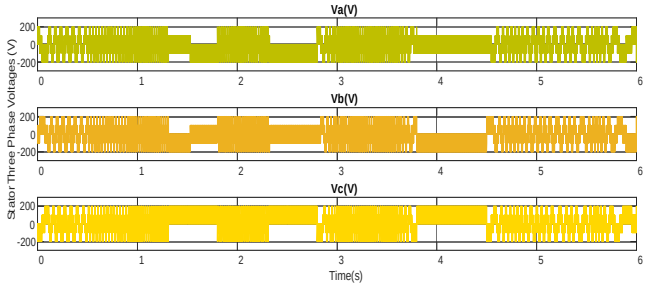

Fig. 22. PMSM three-phase stator voltages

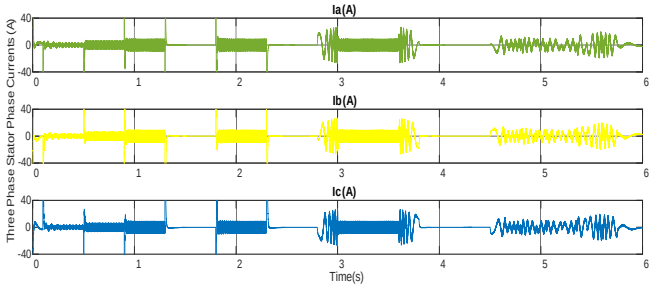

Fig. 23. PMSM three-phase stator currents

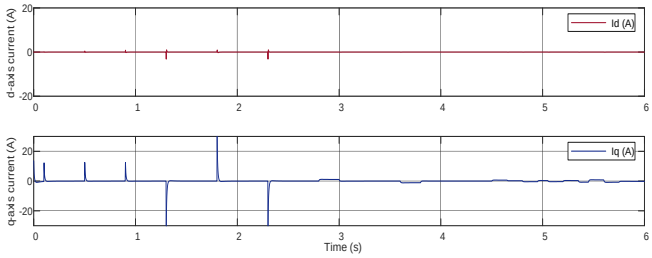

Fig. 24. Quadrature d-axis and q-axis currents

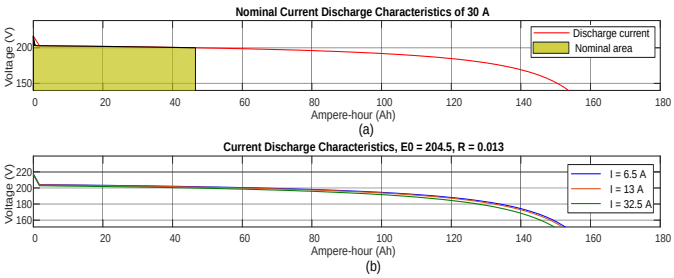

Fig. 25. Battery voltage versus Amp-hour characteristics

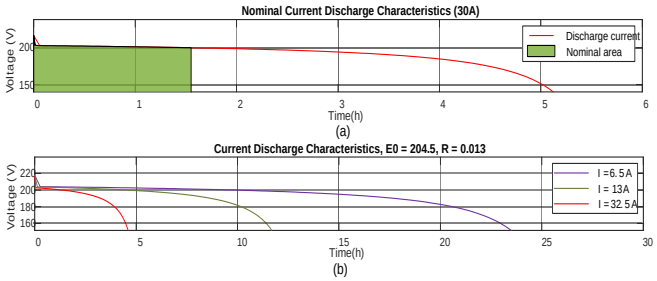

Fig. 26. Battery voltage versus time characteristics

The vehicle and PMSM control strategy aspects have evidently been proven. In actuality, the vehicle speed is expected to be at its desired reference and was achieved. Furthermore, the stator d and q-axis current module responses demonstrate the decoupled functionality of PMSM.

VII. CONCLUSION

In this study, a PEM fuel cell in combination with a boost converter is developed to deliver electric power to a PMSM fed electric vehicle. The indirect vector control of the PMSM mathematical model is designed and simulated. Further, the dynamics of an electric vehicle were considered, and fuzzy PID controller was developed, and the performance was compared with a classical PID controller. The system is tested under constant torque and constant speed mode of operations. The proposed system with a fuzzy PID controller was shown to have a quicker dynamic speed response. Therefore, the proposed system looks to be particularly promising in reliability, static and dynamic responsiveness, efficiency, and performance.

REFERENCES

[1] Vinay. K. M and Isaac Raju, Hybrid Electric Vehicles, International Journal of Engineering Trends and Technology (IJETT), 50(2) (2017) 93-95.

[2] Khaled S. AlQdah, Analysis of the Causes of Hybrid Cars' Rarity in Saudi Arabia. Medina as a Case study, International Journal of Engineering Trends and Technology (IJETT), 68(8) (2020) 62-67.

[3] Chan. C. C, An overview of electric vehicle technology, Proceedings of the IEEE, 81(9) (1993) 1202-1213.

[4] Williams. M. C, Strakey. J. P and Surdoval. W. A, The US department of energy, office of fossil energy stationary fuel cell program, Journal of power sources, 143(1-2) (2005) 191-196.

[5] Gao. L, Dougal. R. A and Liu. S, Active power-sharing in hybrid battery/capacitor power sources, In Eighteenth Annual IEEE Applied Power Electronics Conference and Exposition, 2003, APEC'03, 1 (2003) 497-503. IEEE.

[6] Kim. M. J, Peng. H, Lin. C. C, Stamos. E and Tran. D, Testing, modeling, and control of a fuel cell hybrid vehicle, In Proceedings of 2005, American Control Conference, (2005) 3859-3864. IEEE.

[7] Schofield. N, Yap. H. T and Bingham. C. M, Hybrid energy sources for electric and fuel cell vehicle propulsion, In 2005 IEEE Vehicle Power and Propulsion Conference, (2005) 522-529. IEEE.

[8] Rodríguez. C, M. B, Paleta. M. A. R, Marquez. J. A. R, Pachuca. B. A and de la Vega. J. R. G. Effect of a Rigid Gas Diffusion Media Applied as Distributor of Reagents in a PEMFC in Operation, Part I: Dry Gases, In Int. J. Electrochem. Sci, 4 (2009) 1754-1769.

[9] Yu. X, Zhou. B and Sobiesiak. A Water and thermal management for Ballard PEM fuel cell stack, Journal of Power sources, 147(1-2) (2005) 184-195.

[10] Lin. R, Weng. Y, Lin. X and Xiong. F, Rapid cold start of proton exchange membrane fuel cells by the printed circuit board technology, International journal of hydrogen energy, 39(32) (2014) 18369-18378.

[11] Ettihir. K, Boulon. L, Becher. M, Agbossou. K and Ramadan. H. S, Online identification of semi-empirical model parameters for PEMFCs, International journal of hydrogen energy, 39(36) (2014) 21165-21176.

[12] Yu. Y, Li. H, Wang. H, Yuan. X. Z, Wang. G and Pan. M. U, A review on performance degradation of proton exchange membrane fuel cells during startup and shutdown processes: Causes, consequences, and mitigation strategies, Journal of Power Sources, 205 (2012) 10-23.

[13] Chen. M and Rincon-Mora. G. A, Accurate electrical battery model capable of predicting runtime and IV performance, IEEE transactions on energy conversion, 21(2) (2006) 504-511.
[14] Poushali Pal, Devabalaji K. R and S. Priyadarshini, Design of Battery management system for Residential applications, International Journal of Engineering Trends and Technology (IJETT), 68(3) (2020) 12-17.
[15] Dai. Y, Song. L and Cui. S, Development of PMSM drives for hybrid electric car applications, IEEE transactions on magnetics, 43(1) (2006) 434-437.
[16] Pranoti. G and A. A. Bhole, Integrated Starter Alternator using PMSM, International Journal of Engineering Trends and Technology (IJETT), 62(2) (2019) 113-117.
[17] Chin. Y. K and Soulard. J, A permanent magnet synchronous motor for traction applications of electric vehicles, In IEEE International Electric Machines and Drives Conference, 2003, IEMDC'03.2, (2003) 1035-1041. IEEE.
[18] Bose. B. K, Modern power electronics and AC drives, Upper Saddle River, NJ: Prentice hall. 123 (2002).
[19] Krishnan. R, Permanent magnet synchronous and brushless DC motor drives, CRC press. (2017).
[20] Temitayo O. Olowu, Funso K. Ariyo and Moses O. Onibonoje, Performance Analysis of Direct Torque Controlled, Inverter-fed PMSM Drive for Wire Drawing Machines, International Journal of Engineering Trends and Technology (IJETT), 55(1) (2018) 8-15.
[21] Mohan. N, Advanced electric drives: analysis, control, and modeling using MATLAB/Simulink. John wiley & sons. (2014).
[22] K. Mounika and B. Kiran Babu, Sinusoidal and Space Vector Pulse Width Modulation for Inverter, International Journal of Engineering Trends and Technology (IJETT), 4(4) (2013) 1012-1017.
[23] Swagata Banerjee and Biswamoy Pal, Two Level Inverter Based on Space Vector Pulse Width Modulation Technique, International Journal of Engineering Trends and Technology (IJETT), 22(6) (2015) 265-269.
[24] Wang. S, Shi. Y and Feng. Z, Research on control method based on fuzzy PID controller [J], Mechanical Science and Technology, 30(1) (2011) 166-172.
[25] ZHANG Tao ZHANG Xiao-jiang. L. U and Yu-long. W. L. Y, Research of PMSM Vector Control System Based on Fuzzy Self-tuning PID, Microcomputer Information, 10 (2012).
[26] Liu. J, Advanced PID control and MATLAB simulation, Beijing: Publishing House of electronics industry, 9 (2004).
[27] Thounthong. P, Raël. S and Davat. B, Control strategy of fuel cell/supercapacitors hybrid power sources for electric vehicle. Journal of Power Sources, 158(1) (2006) 806-814.
[28] Lukic. S. M, Cao. J, Bansal. R. C, Rodriguez. F and Emadi. A, Energy storage systems for automotive applications. IEEE Transactions on industrial electronics, 55(6) (2008) 2258-2267.
[29] Hilairet. M, Ghanes. M, Béthoux. O, Tanasa. V, Barbot. J. P and Normand-Cyrot. D, A passivity-based controller for coordination of converters in a fuel cell system. Control engineering practice, 21(8) (2013) 1097-1109.
[30] Tremblay. O and Dessaint. L. A, A generic fuel cell model for the simulation of fuel cell vehicles, In 2009 IEEE vehicle power and propulsion conference, (2009) 1722-1729. IEEE.
[31] Larminie. J, Dicks. A and McDonald. M. S, Fuel cell systems explained, Chichester, UK: J. Wiley. 2 (2003) 207-225.
[32] Dicks. A. L and Rand. D. A, Fuel cell systems explained. John Wiley & Sons. (2018).
[33] Mohan. N, Undeland. T. M and Robbins. W. P, Power electronics: converters, applications, and design. John wiley & sons. (2003).
[34] Lenin. S, Elsa. A, Paola. Q and Henry. A, Design, Construction and Research of an Electric Unicycle with Rechargeable Flow Batteries, International Journal of Engineering Trends and Technology (IJETT), 58(1) (2018) 41-45.
[35] Gharibeh. H. F, Yazdankhah. A. S, Azizian. M. R and Farrokhifar. M, Online Energy Management Strategy for Fuel Cell Hybrid Electric Vehicles with Installed PV on Roof, IEEE Transactions on Industry Applications, 57(3) (2021) 2859-2869.
[36] Nkolika O. Nwazor and Joe Samuel Otonye, Economic Feasibility Analysis of Lithium Ion Batteries for Direct Current Power Supply in Refineries, International Journal of Engineering Trends and Technology (IJETT), 67(3) (2019) 37-43.